

Article

Can DtN and GenEO Coarse Spaces Be Sufficiently Robust for Heterogeneous Helmholtz Problems?

Niall Bootland ^{1,*}  and Victorita Dolean ^{1,2} 

¹ Department of Mathematics and Statistics, University of Strathclyde, Glasgow G1 1XH, UK; victorita.dolean@strath.ac.uk

² Laboratoire J.A. Dieudonné, Centre National de la Recherche Scientifique (CNRS), University Côte d'Azur, 06000 Nice, France

* Correspondence: niall.bootland@strath.ac.uk

Abstract: Numerical solutions of heterogeneous Helmholtz problems present various computational challenges, with descriptive theory remaining out of reach for many popular approaches. Robustness and scalability are key for practical and reliable solvers in large-scale applications, especially for large wave number problems. In this work, we explore the use of a GenEO-type coarse space to build a two-level additive Schwarz method applicable to highly indefinite Helmholtz problems. Through a range of numerical tests on a 2D model problem, discretised by finite elements on pollution-free meshes, we observe robust convergence, iteration counts that do not increase with the wave number, and good scalability of our approach. We further provide results showing a favourable comparison with the DtN coarse space. Our numerical study shows promise that our solver methodology can be effective for challenging heterogeneous applications.

Keywords: Helmholtz equation; domain decomposition; two-level method; coarse space; additive Schwarz method; heterogeneous problem; high frequency



Citation: Bootland, N.; Dolean, V. Can DtN and GenEO Coarse Spaces Be Sufficiently Robust for Heterogeneous Helmholtz Problems? *Math. Comput. Appl.* **2022**, *27*, 35. <https://doi.org/10.3390/mca27030035>

Academic Editor: Eric T. Chung

Received: 17 February 2022

Accepted: 19 April 2022

Published: 21 April 2022

Publisher's Note: MDPI stays neutral with regard to jurisdictional claims in published maps and institutional affiliations.



Copyright: © 2022 by the authors. Licensee MDPI, Basel, Switzerland. This article is an open access article distributed under the terms and conditions of the Creative Commons Attribution (CC BY) license (<https://creativecommons.org/licenses/by/4.0/>).

1. Introduction

Consider solving the heterogeneous Helmholtz problem: for a bounded domain $\Omega \subset \mathbb{R}^d$, $d = 2, 3$, we wish to find $u(x) : \Omega \rightarrow \mathbb{C}$ such that

$$-\Delta u - k^2 u = f \quad \text{in } \Omega, \quad (1a)$$

$$\mathcal{C}(u) = 0 \quad \text{on } \partial\Omega, \quad (1b)$$

where \mathcal{C} incorporates some appropriate boundary conditions. For the heterogeneous problem, we suppose the wave number $k(x) > 0$ is a function of space, defined by the ratio $k = \omega/c$ of the angular frequency ω and the wave speed $c(x)$. In this work, we investigate the use of an overlapping Schwarz preconditioner with a suitably chosen coarse space based on solving local eigenvalue problems on each subdomain.

The ability to compute solutions to the Helmholtz problem (1) is important across many disciplines of science and engineering. As the prototypical model for frequency-domain wave propagation, it features within the fields of optics, acoustics, and seismology, amongst others. Further applications can be found in imaging science, such as through medical imaging techniques and geophysical studies of the Earth's subsurface within, for instance, the oil industry. Nonetheless, it is challenging to develop efficient computational methods to solve (1), particularly when the wave number k becomes large.

Discretisation of (1) by standard approaches, such as Lagrange finite elements, as we shall use here, results in large linear systems to be solved which are indefinite, non-self-adjoint, and ill-conditioned; see also [1]. These systems present various difficulties to solve, especially in the presence of complex heterogeneities, at high frequencies (large k), or when solutions include many wavelengths in the domain. Classical methods for solving

such large systems typically fail for several reasons, as detailed in [2,3], and specialist approaches must be employed for a robust solver. While much progress has been made for symmetric positive definite problems, such techniques cannot be applied out-of-the-box and extensions to tackle indefinite and non-self-adjoint problems may not be clear. This has led to a number of approaches being developed in recent years aiming to bridge this gap. For the Helmholtz problem, this includes parallel direct solvers, such as [4,5], and preconditioned iterative methods that utilise multigrids, such as [6,7], or the so-called “shifted Laplace” approach [8,9]. This latter (complex) shifted Laplace preconditioner has seen much interest into its practical use [10] and further developments through deflation techniques, most recently in [11,12].

Another broad class of solvers are domain decomposition methods, which provide a natural balance between using direct and iterative solvers. Specialist methods are again required for the Helmholtz problem, a popular set of which fall under the heading of “sweeping” methods [13,14]. These are multiplicative domain decomposition methods linked to a variety of other approaches, including optimised Schwarz methods, as detailed in the recent survey [3]. While sweeping is a conceptually serial approach, much work has been done to incorporate parallelism. Of particular note is the “L-Sweeps” method [15], stated to be the first parallel scalable preconditioner for high-frequency Helmholtz problems; a review of developments in this area is provided in the introductions of [15,16]. Other popular approaches are FETI methods; for the Helmholtz problem, these include FETI-H [17] and FETI-DPH [18].

Within the domain decomposition community, there has also been renewed work on additive Schwarz methods, which offer a naturally parallel approach. Following on from the seminal work [19], which utilised Robin (or impedance) transmission conditions to provide a convergent Schwarz method for the Helmholtz problem, a wealth of non-overlapping Schwarz methods have been devised; see the introduction of [20] for a recent overview. In these methods, one has to be careful to either avoid or treat cross points (where three or more subdomains meet), as can be done in the robust treatment of [20]. Many optimised approaches rely on deriving higher-order transmission conditions, such as through second-order impedance operators in [21], absorbing boundary conditions (ABCs) [22], or non-local operators [23]. Ideally, one would use the Dirichlet-to-Neumann (DtN) map (a Poincaré–Steklov operator) to provide transparent transmission conditions, but this is prohibitive in practice, and so these optimised Schwarz methods in essence try to approximate this operator.

Overlapping Schwarz methods for the Helmholtz problem—see for example [24–26]—have also received renewed attention in recent years, and it is this type of method we shall consider. A successful approach is to design additive Schwarz methods based on including absorption (a complex shift $k^2 \mapsto k^2 + i\varepsilon$), with absorption parameter ε ; see [27,28]. Theoretical work to understand the effectiveness of this approach can be found in [29,30] and for the heterogeneous problem in [31]; see also [32]. To be scalable, such additive Schwarz methods require a second level, known as a coarse space (see [33] for a novel analysis for the absorptive problem). For the two-level methods in [27,29], this is provided through a coarse grid—an approach that is effective also for the time-harmonic Maxwell problem [34].

As well as to provide scalability, coarse spaces have been devised to provide robustness to heterogeneity. This is exemplified by the “Generalised Eigenproblems in the Overlap” (GenEO) approach for symmetric positive definite (SPD) problems [35]. This approach provides a spectral coarse space, where appropriate local eigenvalue problems are solved to provide a two-level method. Another spectral coarse space is the DtN coarse space [36], which has been extended and investigated for the Helmholtz problem in [37,38]. While the standard GenEO theory applies only in the SPD case (see [39]), in this work, we develop and explore a GenEO-type method for the Helmholtz problem and show numerically that, for a 2D model problem of a wave guide, it provides a scalable approach that is robust to heterogeneity and increasing wave number in terms of the iteration count of a

preconditioned GMRES method. Companion results for large benchmark problems on coarsely resolved meshes that typically arise in applications, along with comparisons to other methods, are found in [40]. Theoretical results on variants of DtN and GenEO for Helmholtz problems are currently out of reach, but promising numerical results, based on heuristics, were obtained in [37,38], showing the potential of these methods in practice.

The primary aim of this work is to explore the utility of a GenEO-type method for the heterogeneous Helmholtz problem (1); we call this approach H-GenEO. In particular, we highlight the following contributions:

- We present a range of numerical tests, on pollution-free meshes, comparing our proposed H-GenEO approach with another spectral coarse space applicable to the Helmholtz problem, namely the DtN method.
- We investigate the use of appropriate thresholding for the required generalised eigenproblems in both the DtN and H-GenEO coarse spaces.
- We consider robustness to non-uniform decomposition, heterogeneity, and increasing wave number as well as the scalability of the methods. We find that only the H-GenEO approach is scalable and robust to all of these factors for a 2D model problem.
- We provide both weak and strong scalability tests for H-GenEO applied to high wave number problems.

The remainder of this work is structured as follows. We begin by considering a finite element discretisation of the Helmholtz problem in Section 2.1, before outlining the underlying domain decomposition methodology we use in Section 2.2. The main topic of interest, that of suitable spectral coarse spaces for the heterogeneous Helmholtz problem, is then detailed in Section 2.3. Extensive numerical results on a 2D model problem are provided in Section 3, along with a discussion of our findings. Finally, we draw our conclusions in Section 4.

2. Materials and Methods

2.1. Finite Element Discretisation

The problem we consider in this work is the interior Helmholtz problem (1), for which we must prescribe appropriate boundary conditions. In practical applications, the computational domain Ω is often truncated, and the physically relevant condition, namely the far field Sommerfeld radiation condition, must be approximated on the non-physical boundary of Ω . This allows for appropriate wave behaviour to be modelled in a bounded domain. This simplest approximation that is widely used is that of a Robin (or impedance) condition, and this is what we shall consider; other approaches include ABCs [41] or perfectly matched layers (PML) [42,43]. We also suppose that Dirichlet conditions may be imposed on a boundary $\Gamma_D \subset \partial\Omega$, with the Robin condition on the remaining boundary $\Gamma_R = \partial\Omega \setminus \Gamma_D$. Thus, in general, we seek the solution of the boundary value problem

$$-\Delta u - k^2 u = f \quad \text{in } \Omega, \tag{2a}$$

$$u = u_{\Gamma_D} \quad \text{on } \Gamma_D, \tag{2b}$$

$$\frac{\partial u}{\partial \mathbf{n}} + iku = 0 \quad \text{on } \Gamma_R, \tag{2c}$$

where the forcing function $f(x)$ incorporates any sources in the domain. Note that if $\Gamma_R \neq \emptyset$, the problem is well posed, but if $\Gamma_R = \emptyset$, the problem is ill-posed for certain choices of k related to eigenfunctions of the Laplacian.

To discretise (2), we use standard Lagrange finite elements; the details can be found in, for example, [40], and so we provide only an outline here. Defining the relevant trial and test spaces $V = \{u \in H^1(\Omega) : u = u_{\Gamma_D} \text{ on } \Gamma_D\}$ and $V_0 = \{u \in H^1(\Omega) : u = 0 \text{ on } \Gamma_D\}$, the weak formulation of (2) is to find $u \in V$ such that

$$a(u, v) = F(v) \quad \forall v \in V_0, \tag{3}$$

where

$$a(u, v) = \int_{\Omega} (\nabla u \cdot \nabla \bar{v} - k^2 u \bar{v}) \, dx + \int_{\Gamma_R} iku \bar{v} \, ds \quad \text{and} \quad F(v) = \int_{\Omega} f \bar{v} \, dx. \quad (4)$$

Assuming a simplicial mesh \mathcal{T}^h of Ω with characteristic element diameter h , piecewise polynomial finite element approximation reduces the problem to solving the complex linear system

$$A\mathbf{u} = \mathbf{f}, \quad (5)$$

with coefficient matrix $A \in \mathbb{C}^{n \times n}$ and right-hand side vector $\mathbf{f} \in \mathbb{C}^n$ stemming from $a(\cdot, \cdot)$ and $F(\cdot)$, respectively; see [40]. For accurate discretisation of the Helmholtz problem, the number of degrees of freedom n is required to be large, especially for large k . Indeed, to maintain the same level of accuracy of discrete solutions as k increases, the number of mesh points must increase faster than k , due to the pollution effect [44]. This depends on the polynomial order of the approximation used: for instance, using piecewise linear (P1) finite elements, $k^3 h^2$ must be bounded, and so h must shrink as $\mathcal{O}(k^{-3/2})$. Higher order finite elements can reduce this restriction on h , but ultimately the interpolation properties of such methods degrade. Here, we utilise standard P1 elements and maintain a discretisation such that $k^3 h^2$ is fixed to avoid the pollution effect.

2.2. Underlying Domain Decomposition Method

To solve the discrete Helmholtz problem (5), we use GMRES accelerated via a two-level overlapping domain decomposition preconditioner. For the underlying one-level method, we consider the optimised restricted additive Schwarz (ORAS) method [45] (sometimes known as WRAS-H [26]; see discussions in [31,32] and [27,29] for a related IMPHRAS1 method). The key difference in ORAS compared with standard additive Schwarz methods such as RAS is that the local Dirichlet problems on subdomains are replaced by appropriate Robin problems.

To formulate the domain decomposition preconditioner, we first suppose that Ω is decomposed into non-overlapping subdomains $\{\Omega'_s\}_{s=1}^N$, assumed to be resolved by the mesh \mathcal{T}^h . To give an overlapping decomposition, a layer of adjoining mesh elements is added to give overlapping subdomains $\{\Omega_s\}_{s=1}^N$ by way of the extension

$$\Omega_s = \text{Int} \left(\bigcup_{\text{supp}(\phi_j) \cap \Omega'_s \neq \emptyset} \text{supp}(\phi_j) \right), \quad (6)$$

where $\{\phi_j\}_{j=1}^n$ are the nodal basis functions of the finite element space, $\text{Int}(\cdot)$ denotes the interior of a domain, and $\text{supp}(\cdot)$ is the support of a function. Further layers of elements can be added in a recursive manner in order to obtain subdomains with larger overlap, if desired.

Once we have an overlapping decomposition into subdomains $\{\Omega_s\}_{s=1}^N$, we define the required operators for the Schwarz preconditioner. We let $R_s \in \mathbb{R}^{n_s \times n}$ be the discrete form of the restriction operator, restricting functions to the subdomain Ω_s , where n_s is the number of degrees of freedom in Ω_s . The corresponding extension operator, R_s^T , then acts as an extension by zero outside of Ω_s . We also utilise a partition of unity, with the discrete form of a diagonal matrix $D_s \in \mathbb{R}^{n_s \times n_s}$ satisfying $\sum_{s=1}^N R_s^T D_s R_s = I$, which appropriately

scales the multiple subdomain contributions in the overlapping regions. Finally, within ORAS, we require the solution of local Robin problems given by

$$-\Delta w_s - k^2 w_s = f \quad \text{in } \Omega_s, \tag{7a}$$

$$\frac{\partial w_s}{\partial n_s} + ikw_s = 0 \quad \text{on } \partial\Omega_s \setminus \partial\Omega, \tag{7b}$$

$$\mathcal{C}(w_s) = 0 \quad \text{on } \partial\Omega_s \cap \partial\Omega, \tag{7c}$$

with \mathcal{C} representing the underlying problem boundary conditions on $\partial\Omega$, namely (2b) and (2c). Note that the use of the Robin condition (7b) ensures the solvability of these local problems. Defining the equivalent finite element discretisation of (7) to be given by the stiffness matrix $\hat{A}_s \in \mathbb{R}^{n_s \times n_s}$, the construction of the one-level ORAS preconditioner is given by the sum

$$M_{\text{ORAS}}^{-1} = \sum_{s=1}^N R_s^T D_s \hat{A}_s^{-1} R_s. \tag{8}$$

Note that the local solutions on each subdomain given by \hat{A}_s^{-1} can be carried out in parallel.

In order to provide robustness and scalability, the ORAS method above must be augmented by the use of a coarse space to provide a two-level method. A coarse space can be thought of as a collection of linearly independent column vectors Z . The vectors that are incorporated into Z are key to providing scalability, especially for indefinite problems, such as the Helmholtz problems we solve here, where the addition of a coarse space need not improve the performance of the underlying one-level method [46]. There are several ways to incorporate the coarse space; here, we consider an effective approach that is based on deflation. For this, a coarse space operator $E = Z^\dagger A Z$ is constructed as well as the coarse correction operator $Q = Z E^{-1} Z^\dagger$, which we incorporate to give a two-level ORAS method

$$M_{\text{ORAS},2}^{-1} = M_{\text{ORAS}}^{-1} (I - A Q) + Q. \tag{9}$$

We now turn our attention the choice of coarse space.

2.3. Spectral Coarse Spaces

In this work, we consider and explore spectral coarse spaces for the discrete Helmholtz problem (5). These utilise local eigenvalue problems on subdomains in order to build a global coarse space. We review the DtN coarse space [38] before detailing a new coarse space for Helmholtz problems based on GenEO technology [35]. We then show a link between these two approaches.

Remark 1 (Notation). *We utilise the following notation for local Dirichlet, Robin, and Neumann matrices: for a variational problem that gives rise to a system matrix B , we denote by B_s the corresponding local Dirichlet matrix on Ω_s . In the case that Robin conditions are used on internal subdomain interfaces, the local problem matrix is denoted by \hat{B}_s . On the other hand, if Neumann conditions are used on such interfaces, we denote the local matrix by \tilde{B}_s .*

2.3.1. The DtN Coarse Space

The Dirichlet-to-Neumann (DtN) coarse space, first studied in [36,47] for elliptic problems, is based on solving local eigenvalue problems on subdomain boundaries related to a DtN map. Harmonic extensions of low-frequency modes on subdomains are then used to provide a coarse space. In order to define this approach for the Helmholtz problem, as explored in [38], we first require the Helmholtz extension operator from the subdomain boundary $\partial\Omega_s$.

On each subdomain, let $\Gamma_s = \partial\Omega_s \setminus \partial\Omega$, and suppose we have Dirichlet data v_{Γ_s} on Γ_s . The Helmholtz extension v into Ω_s is given by solving

$$-\Delta v - k^2 v = 0 \quad \text{in } \Omega_s, \tag{10a}$$

$$v = v_{\Gamma_s} \quad \text{on } \Gamma_s, \tag{10b}$$

$$\mathcal{C}(v) = 0 \quad \text{on } \partial\Omega_s \cap \partial\Omega, \tag{10c}$$

where $\mathcal{C}(v) = 0$ represents the original problem boundary conditions, as in (7c). The DtN map takes Dirichlet data v_{Γ_s} to the corresponding Neumann data on Γ_s , namely

$$\text{DtN}_{\Omega_s}(v_{\Gamma_s}) = \left. \frac{\partial v}{\partial n} \right|_{\Gamma_s} \tag{11}$$

where v is the Helmholtz extension defined by (10). The associated local DtN eigenproblem on subdomain Ω_s is given by

$$\text{DtN}_{\Omega_s}(u_{\Gamma_s}) = \lambda u_{\Gamma_s}, \tag{12}$$

for eigenfunctions u_{Γ_s} and eigenvalues $\lambda \in \mathbb{C}$. In order to build the coarse space, we take the Helmholtz extension of u_{Γ_s} in Ω_s and extend by zero into the whole domain Ω using the partition of unity; see [38].

To formulate the discrete version of the eigenproblems to be solved, we require the coefficient matrices \tilde{A}_s , corresponding to local Neumann problems on Ω_s with boundary conditions $\mathcal{C} = 0$ on $\partial\Omega_s \cap \partial\Omega$, similar to that supplying the local Robin problems in (7). Furthermore, we must distinguish between degrees of freedom on the boundary and the interior of the subdomain Ω_s , and so we let Γ_s and I_s be the set of indices on the boundary and interior, respectively. Recalling that $\{\phi_j\}$ are our nodal basis functions, we also define

$$M_{\Gamma_s} = \left(\int_{\Gamma_s} \phi_j \phi_i \right)_{i,j \in \Gamma_s} \tag{13}$$

to be the mass matrix on the subdomain interface. Using standard block notation to denote submatrices of A_s and \tilde{A}_s , the discrete DtN eigenproblem can be written as

$$\left(\tilde{A}_{\Gamma_s, \Gamma_s} - A_{\Gamma_s, I_s} A_{I_s, I_s}^{-1} A_{I_s, \Gamma_s} \right) \mathbf{u}_{\Gamma_s} = \lambda M_{\Gamma_s} \mathbf{u}_{\Gamma_s}. \tag{14}$$

We then make use of the Helmholtz extension of \mathbf{u}_{Γ_s} to degrees of freedom in I_s given by $\mathbf{u}_{I_s} = -A_{I_s, I_s}^{-1} A_{I_s, \Gamma_s} \mathbf{u}_{\Gamma_s}$. Letting \mathbf{u}_s denote the complete local vector representing the Helmholtz extension, the corresponding global vector that enters the coarse space Z is $R_s^T D_s \mathbf{u}_s$. Further motivation and details on the DtN eigenproblems can be found in [38].

What remains is to determine which eigenvectors of (14) should be incorporated into the coarse space. A variety of selection criteria were investigated in [38], which made it clear that the best choice was to select eigenvectors corresponding to eigenvalues with the smallest real part. That is, a threshold on the abscissa $\eta = \text{Re}(\lambda)$ should be used, namely

$$\eta < \eta_{\max}, \tag{15}$$

where η_{\max} depends on $k_s = \max_{\vec{x} \in \Omega_s} k(\vec{x})$. The choice $\eta_{\max} = k_s$ is advocated in [38]; however, we recently showed that taking a slightly larger threshold $\eta_{\max} = k_s^{4/3}$ can be beneficial in certain cases in order to gain robustness to the wave number [37]. Unfortunately, this only occurs for the homogeneous problem with sufficiently uniform subdomains. To construct a more robust coarse space, we build upon the GenEO approach.

2.3.2. The GenEO Coarse Space

The Generalised Eigenproblems in the Overlap (GenEO) coarse space was derived in [35] to provide a rigorously robust approach for symmetric positive definite problems even in the presence of heterogeneities. In recent years, this approach has been extended and used within various settings and applications—for example, [39,45,48,49]; see also the discussion on developments for other spectral coarse spaces in [50].

Within the original derivation [35], the generalised eigenproblems are defined in a variational framework on the assumption that $a(\cdot, \cdot)$ is a symmetric and coercive bilinear form. On a subdomain Ω_s , an overlapping zone Ω_s° is defined as the parts of Ω_s that overlap with another subdomain, and the local eigenproblem

$$a_{\Omega_s}(u, v) = \lambda a_{\Omega_s^\circ}(\Xi_s(u), \Xi_s(v)) \quad \forall v \in V(\Omega_s), \tag{16}$$

is solved for small λ , where Ξ_s represents the action of the partition of unity operator on Ω_s . To be clear, $a_D(\cdot, \cdot)$ represents the underlying variational problem on the domain D with problem boundary conditions on $\partial\Omega$ and natural (“do nothing”) conditions on $\partial D \setminus \partial\Omega$. The eigenproblem (16) provides an appropriate link in order to bound the condition number of the preconditioned operator independently of the heterogeneity and number of subdomains. This bound depends on the smallest eigenvalue λ whose corresponding eigenfunction is not incorporated into the GenEO coarse space. Hence, to achieve a desired rate of convergence, all eigenfunctions corresponding to eigenvalues smaller than a threshold (say, $\lambda < \lambda_{\max}$) must be computed. Alternatively, one may opt in practice to compute a fixed number of eigenfunctions per subdomain and use these in order to accelerate convergence.

The restriction within the right-hand side of (16) to the overlapping zone is not an essential requirement, and alternative formulations can be used. In order to remove the need to track overlap regions, one possibility is to replace Ω_s° with the whole of Ω_s , as in [45,48]. When formulating the discrete eigenproblem, this requires only the local Neumann matrix \tilde{A}_s to be constructed. In this case, we must solve

$$\tilde{A}_s \mathbf{u} = \lambda D_s A_s D_s \mathbf{u}, \tag{17}$$

where $A_s = R_s A R_s^T$ is the local Dirichlet matrix—a sub-matrix of A . As with the DtN method, the vectors which then go into the coarse space Z are $R_s^T D_s \mathbf{u}$. It is this form of the GenEO eigenproblem in (17) that we shall build upon to develop an approach tailored to the heterogeneous Helmholtz problem.

2.3.3. H-GenEO: A GenEO-Type Coarse Space for Helmholtz Problems

In consideration of GenEO approaches for the Helmholtz problem, a key hurdle is the loss of operators that are definite or self-adjoint. While some progress has been made at the theoretical level for closely related problems [39,51], currently available analysis has yet to overcome all the challenges present for the Helmholtz problem, and rigorous justification for a choice of spectral coarse space remains out of reach. The approach taken in [39,51] is to formulate the GenEO eigenproblem for a nearby symmetric positive definite problem, here corresponding to a Laplace problem and hence given the name Δ -GenEO. This problem can be given by setting $k = 0$ in (2) and (4). Letting L_s be the local Dirichlet matrix for this problem in Ω_s and \tilde{L}_s be the equivalent Neumann matrix, the Δ -GenEO eigenproblem is given by

$$\tilde{L}_s \mathbf{u} = \lambda D_s L_s D_s \mathbf{u}. \tag{18}$$

This is a positive (semi-)definite eigenproblem with real non-negative eigenvalues λ and, as such, eigenvectors can be chosen in the standard way using a threshold $\lambda < \lambda_{\max}$. Unfortunately, for the Helmholtz problem, the Δ -GenEO approach can perform rather poorly when k becomes large (see Table 1 in Section 3), as might be anticipated from the

fact that solutions to the Laplace problem differ considerably to those of the Helmholtz problem in this range.

In order to provide an appropriate spectral coarse space for the Helmholtz problem, it stands to reason that a Helmholtz operator must be included. If we try to apply the GenEO eigenproblem (17) as is, with matrices stemming from the Helmholtz bilinear form in (4), we must first note that the problem is non-self-adjoint and, as such, eigenvalues λ are no longer real in general. As a threshold criterion, as with the DtN approach, we can consider the abscissa $\eta = \text{Re}(\lambda)$ instead and seek eigenvectors corresponding to $\eta < \eta_{\max}$. Unfortunately, this formulation fails to be robust, and numerically, we have found that the eigensolver we use can often break down. Given that, without any relevant theory, it is no longer clear that (17) provides an appropriate eigenproblem; thus, we develop a different approach that yields a robust method in our numerical experiments.

While the above approaches consider only Helmholtz, or only Laplace, operators in their formulation, we instead link the underlying Helmholtz problem to the positive definite Laplace problem. Since this GenEO-type method targets the Helmholtz problem, we call it ‘‘H-GenEO’’. The local eigenproblem utilised is given by

$$\tilde{A}_s \mathbf{u} = \lambda D_s L_s D_s \mathbf{u}. \tag{19}$$

Since eigenvalues are complex (though, in our experience, they tend to cluster close to the real line) we threshold based on the abscissa $\eta < \eta_{\max}$. We see the effectiveness of the H-GenEO coarse space for a 2D model problem in Section 3. When used with a threshold (typically, we use $\eta_{\max} = \frac{1}{2}$), we observe that the number of GMRES iterations for the H-GenEO approach is independent of the wave number k , which is not true of the DtN method in general. Before continuing to our numerical results, we first show a link between the DtN and GenEO eigenproblems and how the H-GenEO method is related.

2.3.4. A Link between DtN and GenEO

While the DtN and GenEO eigenproblems look rather different, here we show a link between the two approaches. In particular, consider the GenEO method when we remove the partition of unity matrices D_s from (17), so that we are left with the Neumann matrix on the left and the Dirichlet matrix on the right, namely $\tilde{A}_s \mathbf{u} = \lambda A_s \mathbf{u}$. Further, let us use subscripts O_s and I_s to denote overlap and interior degrees of freedom in Ω_s , respectively. Then, moving all terms to the left-hand side, the GenEO eigenproblem can be written as

$$\begin{pmatrix} \tilde{A}_{O_s, O_s} - \lambda A_{O_s, O_s} & (1 - \lambda) A_{O_s, I_s} \\ (1 - \lambda) A_{I_s, O_s} & (1 - \lambda) A_{I_s, I_s} \end{pmatrix} \begin{pmatrix} \mathbf{u}_{O_s} \\ \mathbf{u}_{I_s} \end{pmatrix} = \begin{pmatrix} \mathbf{0} \\ \mathbf{0} \end{pmatrix}, \tag{20}$$

where we have used the fact that the Neumann matrix is equal to Dirichlet matrix except in the block associated with the overlap degrees of freedom. Forming the Schur complement of (20) with respect to the A_{I_s, I_s} block and dividing by $1 - \lambda$, we obtain

$$\left(\tilde{A}_{O_s, O_s} - A_{O_s, I_s} A_{I_s, I_s}^{-1} A_{I_s, O_s} \right) \mathbf{u}_{O_s} = \frac{\lambda}{1 - \lambda} \left(A_{O_s, O_s} - \tilde{A}_{O_s, O_s} \right) \mathbf{u}_{O_s}. \tag{21}$$

Now, if the overlap degrees of freedom O_s are precisely those used as boundary degrees of freedom Γ_s in the DtN method, we see that (21) resembles the DtN eigenproblem (14). The primary difference stems from the right-hand side, where we now have the difference between the Dirichlet and Neumann matrices on the boundary degrees of freedom as opposed to a mass matrix, though we note that these can coincide for certain choices of discretisation; for example, a simple finite difference scheme on a Cartesian grid where forward or backward differences are used to approximate the Neumann condition. The other difference, aside from the partition of unity in the true GenEO approach, stems from a transformation of the eigenvalues, namely the comparative eigenvalues for the DtN method are $\mu = \frac{\lambda}{1 - \lambda}$.

Now consider the H-GenEO eigenproblem (19) without the partition of unity matrices. Splitting for the moment $A = L - k^2M$, we have

$$\begin{pmatrix} \tilde{L}_{O_s,O_s} - \lambda L_{O_s,O_s} - k^2 M_{O_s,O_s} & (1 - \lambda)L_{O_s,I_s} - k^2 M_{O_s,I_s} \\ (1 - \lambda)L_{I_s,O_s} - k^2 M_{I_s,O_s} & (1 - \lambda)L_{I_s,I_s} - k^2 M_{I_s,I_s} \end{pmatrix} \begin{pmatrix} \mathbf{u}_{O_s} \\ \mathbf{u}_{I_s} \end{pmatrix} = \begin{pmatrix} \mathbf{0} \\ \mathbf{0} \end{pmatrix}. \tag{22}$$

Now, dividing by $1 - \lambda$ and defining $\kappa^2 = \frac{k^2}{1-\lambda}$ and the corresponding Helmholtz matrices with wave number κ as $B = L - \kappa^2M$, we have

$$\begin{pmatrix} \tilde{B}_{O_s,O_s} + \frac{\lambda}{1-\lambda}(\tilde{L}_{O_s,O_s} - L_{O_s,O_s}) & B_{O_s,I_s} \\ B_{I_s,O_s} & B_{I_s,I_s} \end{pmatrix} \begin{pmatrix} \mathbf{u}_{O_s} \\ \mathbf{u}_{I_s} \end{pmatrix} = \begin{pmatrix} \mathbf{0} \\ \mathbf{0} \end{pmatrix}. \tag{23}$$

Using the fact that $\tilde{L}_{O_s,O_s} - L_{O_s,O_s} = \tilde{B}_{O_s,O_s} - B_{O_s,O_s}$, the resulting Schur complement system is then given as

$$\left(\tilde{B}_{O_s,O_s} - B_{O_s,I_s} B_{I_s,I_s}^{-1} B_{I_s,O_s} \right) \mathbf{u}_{O_s} = \frac{\lambda}{1-\lambda} \left(B_{O_s,O_s} - \tilde{B}_{O_s,O_s} \right) \mathbf{u}_{O_s}. \tag{24}$$

Thus, we see that H-GenEO corresponds to solving GenEO problems based on a wave number κ that varies with the eigenvalue. Since we are predominantly looking for small eigenvalues λ , this wave number $\kappa = k(1 - \lambda)^{-1/2}$ will then be close to k .

To further exhibit the link between these spectral coarse spaces for the Helmholtz problem, we consider example eigenfunctions for both the DtN (14) and H-GenEO (19) eigenproblems on the central subdomain of a 5×5 decomposition into square subdomains for a homogeneous model problem with $k = 46.5$ (see Section 3 for details). Figure 1 displays a selection of eigenfunctions, and in the top two rows, we plot DtN (top row) and H-GenEO (middle row) eigenfunctions, which show the same features, visually being very similar. Note that, since the central subdomain does not touch the Robin boundary Γ_R , both eigenproblems are real and symmetric, albeit indefinite, and so all eigenvalues λ are real. With DtN, as λ increases, variation in the eigenfunctions tends to be restricted to the boundary, as can be seen in Figure 1c,e. Such behaviour is observed for many H-GenEO eigenfunction as well; however, we also obtain distinct eigenfunctions which are not found amongst DtN eigenfunctions: examples are given in the bottom row of Figure 1, and we note that they tend to exhibit large variation in the interior of the subdomain. Nonetheless, there is a clear link between many of the DtN and H-GenEO eigenfunctions.

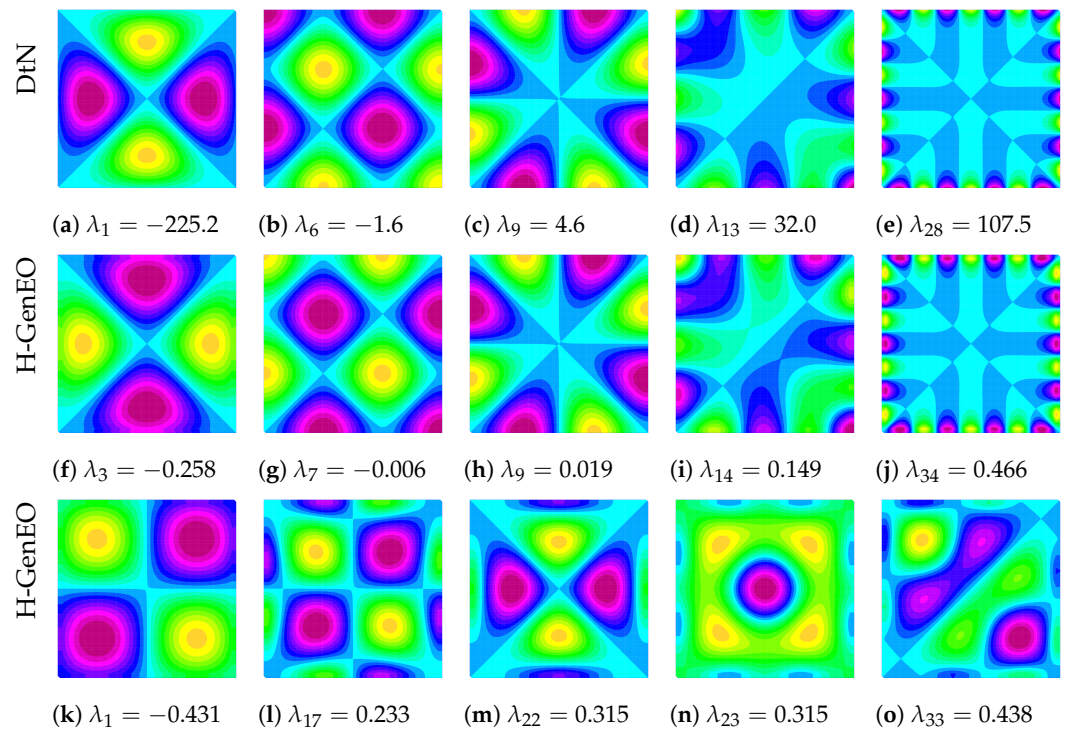


Figure 1. Local eigenfunctions for $k = 46.5$. **Top row:** Examples using DtN (14). **Middle row:** Equivalent examples using H-GenEO (19). **Bottom row:** Examples using H-GenEO which are not found amongst the DtN eigenfunctions.

3. Results and Discussion

In this section, we present and discuss the numerical results computed using FreeFEM [52], in particular through the functionality of `ffddm`, which handles the underlying domain decomposition data structures. As a model problem, we consider the case of a wave guide in 2D, defined on the unit square $\Omega = (0, 1)^2$. We impose homogeneous Dirichlet conditions on two opposite sides, namely (2b) with $u_{\Gamma_D} = 0$ on $\Gamma_D = \{0, 1\} \times [0, 1]$, and Robin conditions on the two remaining sides, that is (2c) on $\Gamma_R = [0, 1] \times \{0, 1\}$. A point source is located in the centre of the domain at $(\frac{1}{2}, \frac{1}{2})$ and provides the forcing function f . A schematic of this model problem is found in Figure 2.

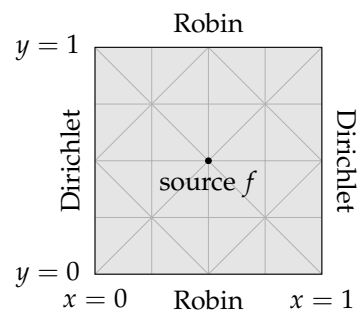


Figure 2. Schematic of the 2D wave guide model problem with example triangular mesh.

To discretise the problem, we triangulate Ω using a Cartesian grid with spacing h and alternating diagonals to form a simplicial mesh (see Figure 2 where $h = \frac{1}{4}$). The discrete problem (5) is then built using a P1 finite element approximation on this mesh. In order to avoid the pollution effect, we choose k and h simultaneously so that $k^3 h^2 = \frac{2\pi}{10}$ is fixed. The large sparse linear system (5) is solved using right-preconditioned GMRES, with the preconditioner given by the two-level ORAS method (9) and the choice of coarse space as stated. We terminate the GMRES iteration once a relative residual tolerance of 10^{-6} is reached. Unless otherwise stated, within the domain decomposition preconditioner, we

use minimal overlap: that is, one layer of adjoining mesh elements are added to the non-overlapping subdomains via the extension in (6). To solve the local eigenvalue problems in the two-level methods, we make use of ARPACK [53], while both the subdomain solves and coarse space operator solves are given by MUMPS [54].

We first compare coarse spaces in the simplest case of a homogeneous problem, investigating the choice of eigenvalue threshold used. We then show results on how the methods perform in a variety of settings; for instance, with non-uniform subdomains, heterogeneity, and additional overlap. Finally, both weak and strong scalability tests are performed for H-GenEO applied to high wave number problems with timings reported.

3.1. A Comparison of Methods for the Homogeneous Problem with Uniform Partitioning

In Table 1, we give some benchmark results for the simplest problem of a homogeneous wave guide using a uniform decomposition into 25 square subdomains. We see that the one-level ORAS method (8) performs relatively poorly as the wave number k increases. The standard DtN coarse space (14) (with $\eta_{\max} = k$) is able to reduce iteration counts with a relatively small coarse space size; however, there is still a clear increase in iterations as k increases. The Δ -GenEO method (18), with $\lambda_{\max} = \frac{1}{2}$, performs poorly here, often performing worse than the one-level method despite a larger coarse space than the DtN approach; this may be because the impedance conditions from the wave guide problem are not included in the definition of the Δ -GenEO coarse space and so the eigenfunctions are not appropriate here. Finally, the standard H-GenEO method (19) (with $\eta_{\max} = \frac{1}{2}$) performs well and significantly reduces the iteration counts, by a factor of 10 for the largest wave number, and provides robustness to increasing wave number k (in fact, iteration counts tend to decrease with k). We note that the size of the H-GenEO coarse space is larger than the DtN coarse space, and we now explore this further.

Table 1. Preconditioned GMRES iteration counts and size of coarse space (in parentheses) for the homogeneous problem when using ORAS and various coarse spaces. A uniform decomposition into 5×5 square subdomains is used, giving 25 subdomains in total.

k	h^{-1}	One-Level	DtN	Δ -GenEO	H-GenEO
18.5	100	73	19 (147)	53 (135)	21 (164)
29.3	200	97	26 (218)	100 (271)	18 (370)
46.5	400	125	35 (303)	148 (560)	17 (779)
73.8	800	156	42 (502)	220 (1120)	15 (1712)

In Table 2, we provide results for both the DtN and H-GenEO methods with differing eigenvalue thresholds η_{\max} . For DtN, we use the standard threshold $\eta_{\max} = k$, the suggested threshold from [37] $\eta_{\max} = k^{4/3}$, and the larger threshold of $\eta_{\max} = k^{3/2}$. For H-GenEO, we use the standard threshold $\eta_{\max} = \frac{1}{2}$ as well as the weaker thresholds of $\frac{1}{4}$ and $\frac{1}{8}$, the latter giving coarse space sizes more comparable to the standard DtN approach. To differentiate between these methods, we use the notation $\text{DtN}(\eta_{\max})$ and $\text{H-GenEO}(\eta_{\max})$ where η_{\max} is as specified. We notice in Table 2 that increasing the DtN threshold to $\eta_{\max} = k^{4/3}$ significantly improves the iteration counts for this problem so that they are almost independent of k , albeit very slightly growing. Increasing the threshold further only marginally improves the iteration counts, which still grow slightly with k , but at the expense of a coarse space almost twice the size. On the other hand, if we relax the H-GenEO threshold, we start to see higher iteration counts and lose some robustness, but generally iteration counts do not increase with k as they do for the standard DtN method. We note that, for this homogeneous problem, roughly comparable coarse space sizes give approximately similar iteration counts, and so it is primarily the thresholds used in DtN and H-GenEO that dictate the different growth behaviour we observe.

Table 2. Preconditioned GMRES iteration counts and size of coarse space (in parentheses) for the homogeneous problem when using ORAS and the DtN and H-GenEO coarse spaces with varying eigenvalue thresholds. A uniform decomposition into 5×5 square subdomains is used, giving 25 subdomains in total.

k	h^{-1}	DtN (k)	DtN ($k^{4/3}$)	DtN ($k^{3/2}$)	H-GenEO ($\frac{1}{8}$)	H-GenEO ($\frac{1}{4}$)	H-GenEO ($\frac{1}{2}$)
18.5	100	19 (147)	13 (260)	11 (403)	46 (80)	31 (105)	21 (164)
29.3	200	26 (218)	14 (483)	13 (759)	53 (139)	33 (189)	18 (370)
46.5	400	35 (303)	14 (868)	12 (1479)	56 (245)	35 (378)	17 (779)
73.8	800	42 (502)	16 (1588)	15 (2925)	40 (546)	25 (800)	15 (1712)

To explore the growth in the size of the coarse space further, in Figure 3a, we plot coarse space size against the wave number k . From this, we can see that growth for DtN($k^{4/3}$) is approximately proportional to $k^{4/3}$, while for H-GenEO($\frac{1}{2}$), it is around $k^{5/3}$ for our model problem. When the thresholds are relaxed, the precise relationship becomes less clear, but we note that the coarse space sizes grows more slowly with a weaker threshold, especially for the DtN approach. The faster growth seen for DtN($k^{4/3}$) and H-GenEO($\frac{1}{2}$) may help to accommodate the stronger robustness to k observed in the iteration counts of Table 2. These two approaches appear to provide the best trade-off for obtaining a well-behaved method, and so we focus primarily on these approaches, but first we consider the question of scalability.

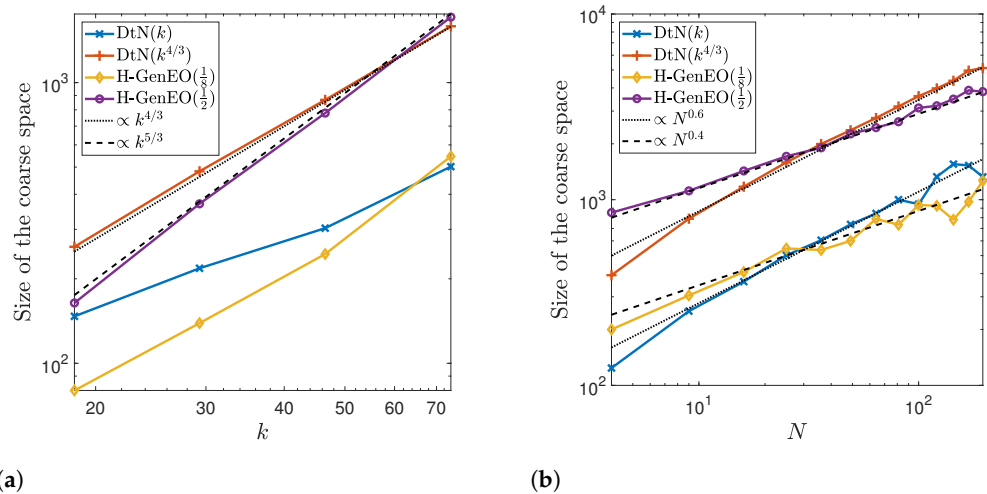


Figure 3. The size of coarse space utilised for the homogeneous problem when using ORAS with the DtN and H-GenEO coarse spaces. A uniform decomposition into $\sqrt{N} \times \sqrt{N}$ square subdomains is used. (a) Varying the wave number k for $N = 25$, (b) Varying the number of subdomains N for $k = 73.8$.

3.2. Scalability of DtN and H-GenEO for the Homogeneous Problem with Uniform Partitioning

We now investigate the scalability of the DtN and H-GenEO methods. This will depend on the threshold used, and so we compare results for DtN(k) and H-GenEO($\frac{1}{8}$) as well as DtN($k^{4/3}$) and H-GenEO($\frac{1}{2}$), with each pair of approaches giving broadly similar iteration counts. Results for the homogeneous problem with $k = 73.8$ and $h^{-1} = 800$ are given in Table 3 for an increasing number of uniform square subdomains N . We see that the DtN(k) approach does not exhibit scalability here, with iteration counts that noticeably increase with N . Similarly, with the weaker threshold, H-GenEO($\frac{1}{8}$) also fails to be scalable. On the other hand, both DtN($k^{4/3}$) and H-GenEO($\frac{1}{2}$) are scalable here, with low iteration counts that vary little with N .

Comparing the size of the coarse spaces employed, we see that the DtN($k^{4/3}$) coarse space grows faster with N and becomes larger than the H-GenEO($\frac{1}{2}$) coarse space, which

may account for its particularly strong robustness to N here. From Figure 3b, we see that for both DtN approaches, the coarse space size grows approximately proportional to $N^{0.6}$, while for the H-GenEO method, it is around $N^{0.4}$. This suggests that H-GenEO may be advantageous when N becomes large due to the smaller coarse space required. For each method, the average number of eigenvectors taken per subdomain decreases as N increases; this means that, as well as smaller subdomain solves, we also benefit from requiring fewer eigenvectors to be computed per subdomain, even if the global coarse space size increases. We note that the size of the DtN(k) or H-GenEO($\frac{1}{8}$) coarse space sometimes shrinks as we increase N , and in these cases, the iteration counts tend to be particularly poor, suggesting that the thresholds of $\eta_{\max} = k$ for DtN and $\eta_{\max} = \frac{1}{8}$ are not doing a suitable job in capturing the eigenfunctions required for scalability. As such, we now narrow our focus to the DtN($k^{4/3}$) and H-GenEO($\frac{1}{2}$) approaches.

Table 3. Preconditioned GMRES iteration counts (above), size of coarse space (middle), and average number of eigenvectors taken per subdomain (below) for the homogeneous problem when using ORAS with the DtN and H-GenEO coarse spaces and a varying number of subdomains N for $k = 73.8$ and $h^{-1} = 800$. A uniform decomposition into $\sqrt{N} \times \sqrt{N}$ square subdomains is used.

N	4	9	16	25	36	49	64	81	100	121	144	169	196
DtN (k)	28	32	40	42	51	76	49	94	90	36	37	96	154
DtN ($k^{4/3}$)	15	16	19	16	16	16	15	16	15	15	16	17	17
H-GenEO ($\frac{1}{8}$)	26	31	36	40	71	70	65	127	81	116	247	194	138
H-GenEO ($\frac{1}{2}$)	13	15	15	15	16	16	16	18	16	18	18	18	19
DtN (k)	124	251	362	502	605	736	843	1000	946	1329	1554	1529	1327
DtN ($k^{4/3}$)	392	790	1175	1588	1994	2366	2753	3176	3611	3976	4369	4955	5118
H-GenEO ($\frac{1}{8}$)	200	305	408	546	536	600	788	733	936	927	780	974	1264
H-GenEO ($\frac{1}{2}$)	852	1116	1428	1712	1903	2261	2444	2629	3120	3204	3482	3882	3816
DtN (k)	31.0	27.9	22.6	20.1	16.8	15.0	13.2	12.3	9.5	11.0	10.8	9.0	6.8
DtN ($k^{4/3}$)	98.0	87.8	73.4	63.5	55.4	48.3	43.0	39.2	36.1	32.9	30.3	29.3	26.1
H-GenEO ($\frac{1}{8}$)	50.0	33.9	25.5	21.8	14.9	12.2	12.3	9.0	9.4	7.7	5.4	5.8	6.4
H-GenEO ($\frac{1}{2}$)	213.0	124.0	89.3	68.5	52.9	46.1	38.2	32.5	31.2	26.5	24.2	23.0	19.5

3.3. Robustness of DtN and H-GenEO for the Homogeneous Problem with METIS Decomposition

We now consider utilising non-uniform subdomains, as provided through the software METIS [55]. In Table 4, we compare DtN($k^{4/3}$) and H-GenEO($\frac{1}{2}$) in this situation, again for the homogeneous problem. We observe that both methods retain their robustness, meaning that iteration counts only depend mildly on the wave number k and the number of subdomains N . For H-GenEO($\frac{1}{2}$), the scalability becomes more favourable for larger k , and we can see that for the smallest wave numbers with large N , the average number of eigenvectors per subdomain becomes very small; in fact, on many subdomains, only a single eigenvector is taken, and so the achieved tolerance on the eigenvalue may be somewhat weaker than $\frac{1}{2}$, which may explain the slightly poorer performance. One way this could be overcome is by always taking a minimum number of eigenvectors per subdomain; for instance, using at least 5 eigenvectors per subdomain when $k = 18.5$ gives iteration counts bounded by 19. Since we are primarily interested in approaches that remain effective for increasingly large wave numbers, where this issue diminishes, we do not worry further about this and assert that for problems of interest, H-GenEO($\frac{1}{2}$) provides good scalability. On the other hand, for DtN($k^{4/3}$), the mild increase in iteration count is seen as k increases here, with scalability observed for all wave numbers.

We note that the coarse space sizes for each method tend to be slightly larger with the more general decompositions used by METIS, but otherwise the same trends are seen. As such, we conclude that non-uniform decompositions can be well handled by the spectral coarse spaces employed here.

Table 4. Preconditioned GMRES iteration counts (above), size of coarse space (middle), and average number of eigenvectors taken per subdomain (below) for the homogeneous problem when using ORAS with DtN($k^{4/3}$) or H-GenEO($\frac{1}{2}$) and a varying number of subdomains. A non-uniform decomposition into N subdomains is used, given by METIS.

k	h^{-1}	Number of Subdomains N											
		DtN ($k^{4/3}$)						H-GenEO ($\frac{1}{2}$)					
		20	40	80	120	160	200	20	40	80	120	160	200
18.5	100	10	10	10	10	10	10	15	17	19	22	27	27
29.3	200	12	15	11	12	12	12	15	17	19	20	22	23
46.5	400	12	13	15	13	13	13	15	16	16	18	20	20
73.8	800	15	15	14	16	14	16	15	16	17	17	17	19
117.2	1600	14	15	16	17	15	16	14	15	15	16	16	16
18.5	100	281	422	652	843	1005	1157	201	285	383	471	524	589
29.3	200	477	758	1130	1410	1693	1922	400	574	783	958	1097	1245
46.5	400	959	1466	2132	2677	3151	3553	869	1193	1670	2008	2253	2507
73.8	800	1695	2563	3751	4672	5486	6199	1863	2456	3433	4147	4749	5338
117.2	1600	3049	4695	6831	8486	9896	11,092	4238	5680	7575	9049	10,273	11,305
18.5	100	14.1	10.6	8.2	7.0	6.3	5.8	10.1	7.1	4.8	3.9	3.3	2.9
29.3	200	23.9	18.9	14.1	11.8	10.6	9.6	20.0	14.3	9.8	8.0	6.9	6.2
46.5	400	48.0	36.6	26.6	22.3	19.7	17.8	43.5	29.8	20.9	16.7	14.1	12.5
73.8	800	84.8	64.1	46.9	38.9	34.3	31.0	93.2	61.4	42.9	34.6	29.7	26.7
117.2	1600	152.4	117.4	85.4	70.7	61.9	55.5	211.9	142.0	94.7	75.4	64.2	56.5

3.4. The Effect of Heterogeneity

We now turn our attention to the key property of robustness to heterogeneities. For this, we consider layered media within the wave guide. Three configurations, each having 10 layers, are used and are detailed in Figure 4. The heterogeneity is introduced in the wave speed $c(x)$, and in each case, c takes values from 1 to ρ , where ρ is a contrast parameter determining the strength of the heterogeneity. The wave number is then given by $k = \omega/c$ where ω is the angular frequency; we vary both ω and ρ in our tests. Note that for the DtN method, the eigenvalue threshold now depends on $k_s = \max_{\vec{x} \in \Omega_s} k(\vec{x})$, which may be different for different subdomains Ω_s . To avoid notational clutter, we omit the subscript when referring to the method, namely retaining the name DtN($k^{4/3}$).

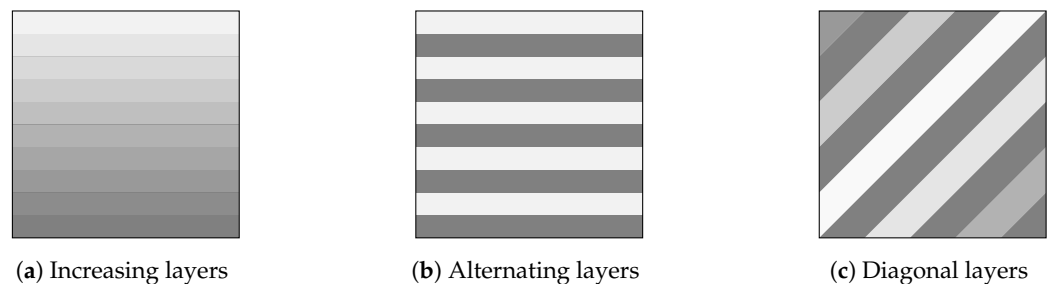


Figure 4. Piecewise constant layer profiles for the wave speed $c(x)$. For the darkest shade $c(x) = 1$, while for the lightest shade $c(x) = \rho$, with ρ being the contrast factor.

Results for DtN($k^{4/3}$) and H-GenEO($\frac{1}{2}$) for the increasing layers problem (Figure 4a) are provided in Table 5. Unfortunately, we see that the DtN($k^{4/3}$) loses robustness with the heterogeneity present in this problem. In particular, we lose any robustness to the wave number k , and for the largest wave number used, we also see that changes in the contrast, given by ρ , can begin to have a sizeable impact on the iteration counts despite otherwise being relatively stable to changes in ρ . To a lesser extent, we also lose scalability with DtN($k^{4/3}$) as the iteration counts now slowly increase with N . On the other hand, H-GenEO($\frac{1}{2}$) has strong robustness throughout, both with respect to the wave number k ,

the contrast in the heterogeneity ρ , and scalability as N increases. As such, we see a clear preference for H-GenEO($\frac{1}{2}$) as a stable and reliable method for heterogeneous problems.

Table 5. Preconditioned GMRES iteration counts (above) and size of coarse space (below) for the heterogeneous increasing layers problem when using ORAS with DtN($k^{4/3}$) or H-GenEO($\frac{1}{2}$) and a varying number of subdomains. A uniform decomposition into $\sqrt{N} \times \sqrt{N}$ square subdomains is used.

ω	h^{-1}	ρ	Number of Subdomains N											
			DtN ($k^{4/3}$)						H-GenEO ($\frac{1}{2}$)					
			16	36	64	100	144	196	16	36	64	100	144	196
29.3	200	10	29	37	41	52	55	58	15	16	19	18	18	19
		1000	44	44	50	58	52	52	15	15	17	18	17	17
46.5	400	10	32	38	41	66	65	73	15	16	16	19	18	18
		1000	63	69	74	84	73	71	14	15	16	18	17	17
73.8	800	10	35	43	42	40	58	69	15	17	16	17	18	17
		1000	89	93	107	111	114	109	14	15	15	16	17	16
29.3	200	10	116	173	234	363	399	467	224	354	452	662	679	754
		1000	84	111	136	285	329	371	222	350	446	642	679	741
46.5	400	10	208	317	405	600	704	812	458	706	990	1234	1523	1678
		1000	144	176	202	421	496	554	450	693	990	1216	1512	1666
73.8	800	10	379	557	693	1142	1217	1404	930	1425	2074	2584	3060	3553
		1000	254	294	326	748	784	838	914	1409	2058	2572	3059	3534

We also consider the case of a diagonal layers problem (Figure 4c) in Table 6. Here, the issues with DtN($k^{4/3}$) are reduced, but there is still some increase in iteration counts, especially for higher wave numbers k and a larger number of subdomains N . We note, in results not shown here, that DtN($k^{3/2}$) also suffers from the same lack of robustness. For H-GenEO($\frac{1}{2}$), however, we still have good robustness to the parameters of the problem.

We further consider the heterogeneous problem when making use of METIS for more general non-uniform subdomain decompositions in order to ensure that H-GenEO is able to handle both difficulties together. For this, we consider the alternating layers problem (Figure 4b) and provide results in Table 7. We find that H-GenEO($\frac{1}{2}$) performs very well and continues to provide a rather robust method, even in the presence of heterogeneity on non-uniform subdomains. This further evidences the strength of the H-GenEO($\frac{1}{2}$) approach, and we briefly study this more closely, dropping reference to the eigenvalue tolerance and simply denoting the method as H-GenEO. First, however, we provide a brief examination into the use of higher order discretisation.

Table 6. Preconditioned GMRES iteration counts (above) and size of coarse space (below) for the heterogeneous diagonal layers problem when using ORAS with DtN($k^{4/3}$) or H-GenEO($\frac{1}{2}$) and a varying number of subdomains. A uniform decomposition into $\sqrt{N} \times \sqrt{N}$ square subdomains is used.

ω	h^{-1}	ρ	Number of Subdomains N											
			DtN ($k^{4/3}$)						H-GenEO ($\frac{1}{2}$)					
			16	36	64	100	144	196	16	36	64	100	144	196
29.3	200	10	13	14	13	14	21	25	16	18	20	18	23	25
		1000	13	14	14	14	22	25	16	18	20	18	23	25
46.5	400	10	15	14	14	16	25	31	16	17	17	26	21	22
		1000	15	14	15	16	25	34	16	17	18	27	22	22
73.8	800	10	14	18	16	15	20	26	16	17	17	17	19	20
		1000	15	18	16	15	32	39	16	17	17	17	19	20
29.3	200	10	336	593	866	1090	1376	1390	260	376	499	689	737	828
		1000	336	594	866	1090	1375	1390	259	375	499	687	737	826
46.5	400	10	621	1075	1540	1910	2370	2622	543	789	1095	1384	1599	1825
		1000	621	1075	1539	1907	2368	2614	541	790	1093	1381	1596	1824
73.8	800	10	1164	1947	2692	3592	4145	4608	1145	1636	2243	2823	3233	3681
		1000	1163	1946	2693	3592	4131	4569	1141	1633	2239	2822	3232	3671

Table 7. Preconditioned GMRES iteration counts for the heterogeneous alternating layers problem with $\rho = 10/100/1000$ when using ORAS with H-GenEO($\frac{1}{2}$) and a varying number of subdomains. A non-uniform decomposition into N subdomains is used, given by METIS.

ω	h^{-1}	Number of Subdomains N with Sub-Columns for $\rho = 10/100/1000$																		
		20	40				80				120				160				200	
18.5	100	17	17	17	19	19	19	21	21	21	27	27	27	31	31	31	33	33	33	
29.3	200	16	16	16	17	17	17	19	19	19	20	20	20	21	21	21	23	23	23	
46.5	400	17	18	18	18	18	18	22	23	23	25	26	26	27	28	28	28	29	29	
73.8	800	16	16	16	17	17	17	18	18	18	18	19	19	19	20	20	23	23	23	
117.2	1600	15	15	15	15	16	16	16	16	16	16	16	16	16	16	16	16	16	16	

3.5. Higher Order Finite Elements

We briefly investigate the use of higher order finite elements. In particular, we consider the use of P2 elements as opposed to P1 elements. To give a direct comparison, we utilise the same meshes, and in Table 8 we give results for the heterogeneous diagonal layers problem with $\rho = 10$; equivalent results for P1 elements are given in Table 6. We observe that both iteration counts and coarse space sizes remain rather similar to the case of P1 elements. This suggests that, by itself, the order of the underlying finite elements used does not strongly affect performance. However, the typical meshes employed for higher order elements may be coarser, and further studies would be required to observe how this affects the utility of the spectral coarse spaces presented here. Further investigation into which method and order of finite element approximation provides the most efficient choice is beyond the scope of the present study.

Table 8. Preconditioned GMRES iteration counts (above) and size of coarse space (below) for P2 finite element discretisation of the heterogeneous diagonal layers problem with $\rho = 10$ when using ORAS with DtN($k^{4/3}$) or H-GenEO($\frac{1}{2}$) and a varying number of subdomains. A uniform decomposition into $\sqrt{N} \times \sqrt{N}$ square subdomains is used.

ω	h^{-1}	ρ	Number of Subdomains N											
			DtN ($k^{4/3}$)						H-GenEO ($\frac{1}{2}$)					
			16	36	64	100	144	196	16	36	64	100	144	196
18.5	100	10	13	11	10	10	10	18	15	16	19	18	23	24
29.3	200	10	14	12	12	13	19	25	15	17	18	18	23	25
46.5	400	10	15	12	12	15	23	30	15	16	17	20	21	22
73.8	800	10	17	16	14	13	18	25	15	16	16	17	18	20
18.5	100	10	151	326	510	706	898	937	125	186	231	346	398	519
29.3	200	10	300	608	892	1086	1444	1516	260	377	507	686	733	824
46.5	400	10	589	1108	1572	2069	2491	2638	540	794	1100	1403	1594	1820
73.8	800	10	919	1916	2862	3614	4409	4748	1144	1645	2239	2805	3225	3695

3.6. The Effect of Boundary Conditions within the H-GenEO Eigenproblem

We now consider the choice of boundary conditions within H-GenEO in light of the fact that, for wave propagation problems, impedance conditions can often prove more practical within overlapping Schwarz methods. To this end, we consider the H-GenEO eigenproblem where the Neumann boundary condition is replaced by an impedance condition instead (i.e., the Robin condition in (7b)). Results for this impedance–H-GenEO method are given in Table 9 for the homogeneous problem with uniform square subdomains. We see that, while the use of this eigenproblem retains the good behaviour of H-GenEO as k increases, it lacks scalability as we increase the number of subdomains N . We note that the size of the coarse space is very similar to that when the standard Neumann condition is used (a direct comparison can be made for $k = 73.8$ with results in Table 3), and so this is not simply an artefact of a smaller coarse space. This shows that the Neumann condition within the eigenproblem is an important aspect of H-GenEO.

Table 9. Preconditioned GMRES iteration counts (above) and size of coarse space (below) for the homogeneous problem when using ORAS with impedance-H-GenEO (the eigenproblem (19) is altered to have impedance as opposed to Neumann boundary conditions on the left-hand side) and a varying number of subdomains. A uniform decomposition into $\sqrt{N} \times \sqrt{N}$ square subdomains is used.

k	h^{-1}	Number of Subdomains N												
		4	9	16	25	36	49	64	81	100	121	144	169	196
18.5	100	17	19	23	27	30	36	42	45	43	58	61	61	67
29.3	200	17	19	22	25	34	33	41	38	35	49	60	62	65
46.5	400	15	18	19	22	26	25	26	39	43	47	52	51	54
73.8	800	15	19	19	20	25	27	26	35	33	39	43	44	51
18.5	100	68	102	140	158	204	217	236	287	344	341	404	477	504
29.3	200	148	215	296	370	392	521	504	576	720	768	725	793	908
46.5	400	360	492	628	754	917	988	1236	1176	1468	1550	1740	1807	1930
73.8	800	848	1106	1420	1696	1877	2218	2432	2574	2960	3180	3443	3834	3732

3.7. The Effect of More Overlap When Using H-GenEO

So far, all our results use minimal overlap. Here, we consider the case of increasing the overlap between subdomains—this is done by adding on layers of adjoining elements to each subdomain in a symmetric way so that minimal overlap is given by an overlap parameter of 2; that is, the overlapping region has a width of 2 elements. In Table 10, we

report results for increasing overlap when using H-GenEO for the homogeneous problem with $k = 46.5$ and $h^{-1} = 400$ and where a uniform decomposition is used. We see that adding on a small amount of overlap can slightly decrease the iteration counts, but increasing the overlap width further can give much poorer results, especially when using a large number of subdomains N . One possible explanation could be an increase in the “colouring constant” (see, e.g., [45] (Definition 5.5)). We note that the size of the coarse space decreases somewhat as the overlap is increased; however, the extra computational effort required to deal with the larger subdomains will hamper any gains from this, along with the increased iteration counts. From these results, we determine that the H-GenEO coarse space is best suited to the case of minimal overlap, as we have used elsewhere throughout this work.

Table 10. Preconditioned GMRES iteration counts (above) and size of coarse space (below) for the homogeneous problem when using ORAS with H-GenEO, varying the amount of overlap (in terms of element width, with 2 representing minimal overlap) and number of subdomains for $k = 46.5$ and $h^{-1} = 400$. A uniform decomposition into $\sqrt{N} \times \sqrt{N}$ square subdomains is used.

Overlap	Number of Subdomains N												
	4	9	16	25	36	49	64	81	100	121	144	169	196
2	14	15	15	17	16	16	16	20	26	19	19	22	21
4	10	11	11	12	12	13	12	17	14	16	17	21	20
8	8	10	10	10	13	13	12	20	23	22	26	31	27
16	13	21	26	26	37	77	61	75	86	109	178	157	164
2	368	492	644	779	938	1030	1248	1195	1476	1558	1758	1845	2016
4	352	472	600	699	871	947	1088	1124	1296	1449	1689	1697	1690
8	336	436	538	650	799	863	1024	981	1132	1395	1511	1425	1512
16	316	417	500	610	733	717	920	942	1108	1239	1086	1212	1280

3.8. Weak Scalability and Timing Results for H-GenEO

In this section, we consider the weak scalability of the H-GenEO method. To approach this, we consider a growing wave guide domain where fixed size subdomains are added, each with the same number of degrees of freedom (dofs). This is done by repeatedly adding a unit square, which is split into 25 non-overlapping square subdomains, to the right of the existing domain L times to give $\Omega = (0, L) \times (0, 1)$. Along the long edges of the global domain, we prescribe homogeneous Dirichlet boundary conditions, while Robin conditions are used at each end of the wave guide; a schematic for this weak scaling test is given in Figure 5. Heterogeneity is given by the alternating layers problem (see Figure 4b) with the 10 layers extending across the length of the wave guide.

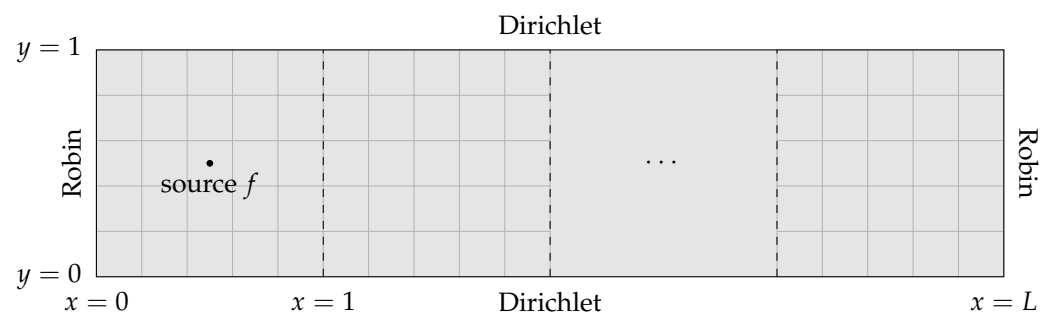


Figure 5. Schematic of the growing 2D wave guide model problem used in a weak scaling test on $N = 25L$ fixed size subdomains, with the underlying non-overlapping subdomains shown in grey.

To deal with the large problem sizes (reaching up to 10,253,601 dofs) and provide appropriate timing results, we assign one core per subdomain and solve using the ARCHIE-WeSt

supercomputing facility on up to 400 cores (the machine uses Intel Xeon Gold 6138 processors at 2.0 GHz with 4.8 GB RAM per core).

In Table 11, we give results for a length of domain $L = 2$ up to $L = 16$; that is, from $N = 50$ to $N = 400$ subdomains, using $k = 73.8$, $h^{-1} = 800$ and $\rho = 100$. We observe that the iteration counts remain almost constant, increasing only very mildly with N . On the other hand, the coarse space size grows linearly with N , as expected given that subdomains have a fixed size, and we see that the time taken to solve the eigenproblems stays constant. However, due the increasing size of the coarse space, the run times slowly increase, meaning that the efficiency degrades as we solve increasingly large problems. Further, the setup of the decomposition and partitioning is performed sequentially, and so this setup time increases with N . Nonetheless, when removing this initial setup, the efficiency still slowly reduces as we increase the problem size, as can be seen in the final row of Table 11. To overcome this, the factorisation of the coarse space operator and associated solves must be made scalable. While a multi-level approach is therefore an attractive option, it is not yet clear how to formulate such a strategy for Helmholtz problems. Additionally, the coarse problem is only assigned to one process here, and so spreading it over more processes as N increases may stop the coarse solve from becoming a bottleneck.

Table 11. Weak scaling results and timings for the alternating layers problem when using ORAS with H-GenEO ($\frac{1}{2}$) and a varying number of subdomains for $k = 73.8$, $h^{-1} = 800$ and $\rho = 100$. A uniform decomposition into $N = 25L$ subdomains is used, as depicted in Figure 5. Note that setup refers to the initial decomposition and partitioning, which is performed sequentially, while the local problems and eigensolves are carried out in parallel.

N	50	100	150	200	250	300	350	400
Iteration count	17	18	18	19	19	20	21	21
Coarse space size	3010	6150	9290	12,430	15,570	18,710	21,850	24,990
Total run time (s)	45.8	48.6	53.0	58.7	63.5	70.0	79.7	88.1
Weak scaling efficiency	—	94.2%	86.4%	78.0%	72.1%	65.4%	57.5%	52.0%
Eigensolve time (s)	37.1	37.9	37.9	38.3	37.8	37.9	37.9	37.7
Setup time (s)	5.5	7.7	12.9	16.5	19.9	23.8	27.4	30.8
Efficiency without setup	—	98.5%	100.5%	95.5%	92.4%	87.2%	77.1%	70.3%

3.9. High Wave Number Strong Scalability and Timing Results for H-GenEO

To conclude our numerical results, we consider the use of H-GenEO within a high wave number example and explore timings and the overall strong scalability of the approach. To this end, we consider the original homogeneous wave guide, as outlined in Figure 2, with a wave number of $k = 186.0$ and mesh width $h^{-1} = 3200$, giving a total problem size of 10,246,401 dofs. To solve, we use METIS to give a non-uniform decomposition into subdomains and again utilise the ARCHIE-WeSt supercomputing facility to assign one core per subdomain.

Results are tabulated in Table 12, in which we detail the run time (in seconds) and the percentage of time spent by the eigensolver and coarse factorisation. The run times are further used to determine the parallel efficiency based on the smallest run on $N = 80$ cores. Timing results are also displayed graphically in Figure 6, where we show that the bulk of the computation is spent in the eigensolves and factorisation of the coarse problem; as such, while the METIS decomposition is sequential, we do not separate out the setup time here, given that it is comparatively rather small. From Table 12, we see that the iteration counts show good scalability, increasing only very mildly as we increase the number of subdomains fivefold. This is also seen in the run times, which decrease as we use more cores, and hence more subdomains, to solve the problem. In particular, we see that the parallel efficiency remains over 100%, showing the strong scalability of the approach, in part due to the fact that as N increases, we have to solve smaller eigenproblems, and so the percentage of time spent by the eigensolver drops significantly as we increase N . Overall,

these provide promising results that the H-GenEO method can be effective for the solution of high wave number problems in 2D.

Table 12. Strong scaling results and timings for the homogeneous problem when using ORAS with H-GenEO ($\frac{1}{2}$) and a varying number of subdomains for $k = 186.0$ and $h^{-1} = 3200$, giving a total of 10,246,401 dofs. A non-uniform decomposition into N subdomains is used, given by METIS. The average local eigenproblem size is given approximately as the number of dofs divided by N .

N	80	120	160	200	240	280	320	360	400
Iteration count	14	16	15	16	17	17	18	19	19
Coarse space size	16,014	19,018	21,348	23,747	25,560	27,270	28,793	30,357	31,773
Total run time (s)	1214.4	614.6	404.4	279.3	217.3	195.0	159.4	154.0	147.6
Parallel efficiency	—	132%	150%	174%	186%	178%	190%	175%	165%
Eigenproblem size (approx.)	128,080	85,387	64,040	51,232	42,693	36,594	32,020	28,462	25,616
Average no. of eigenvectors	200.2	158.5	133.4	118.7	106.5	97.4	90.0	84.3	79.4
Eigensolve time	68.6%	70.1%	66.8%	62.7%	53.7%	52.3%	41.6%	39.3%	37.3%
Coarse factorisation time	29.6%	27.8%	30.8%	34.4%	42.8%	44.3%	54.0%	56.3%	58.3%

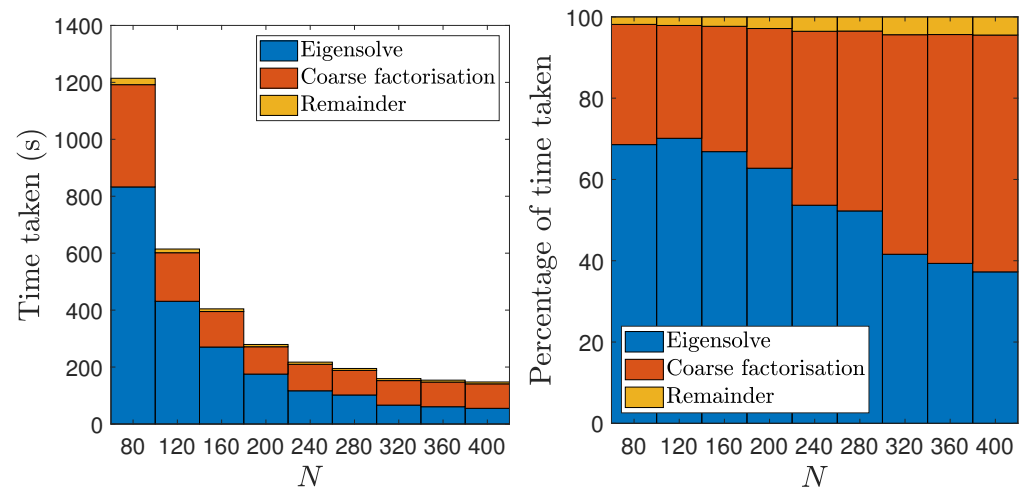


Figure 6. Timings for the homogeneous problem when using ORAS with H-GenEO ($\frac{1}{2}$) and a varying number of subdomains for $k = 186.0$ and $h^{-1} = 3200$, giving a total of 10,246,401 dofs. A non-uniform decomposition into N subdomains is used, given by METIS.

4. Conclusions

In this work, we have developed and explored a GenEO-type coarse space for additive Schwarz methods that is appropriate for the heterogeneous Helmholtz problem. We have conducted extensive numerical tests to show how this approach behaves on a 2D model test problem of a wave guide discretised using finite elements on a pollution-free mesh, comparing our method with the DtN coarse space. We find that only our H-GenEO approach is robust to heterogeneity and increasing wave number k and further provides good scaling such that iteration counts of right-preconditioned GMRES are only mildly dependent on the number of subdomains. This dependence is strongest for lower wave numbers on many subdomains and reduces as k grows. Furthermore, convergence does not deteriorate with increasing wave number, albeit at the cost of a coarse space that grows as k increases. This is achieved consistently for non-uniform partitioning into subdomains and in the presence of strong heterogeneity. These results show promise that H-GenEO can be used as an effective coarse space for challenging heterogeneous problems.

Finally, we discuss how these findings differ from that in the companion paper [40], where none of the approaches (including the spectral coarse spaces explored in detail here) are seen to be clearly favourable over a wide range of problem settings. A key difference

is that well-resolved pollution-free meshes are used in the present work, while the more realistic benchmark problems examined in [40] use under-resolved meshes with a fixed number of points per wavelength, as is typical in engineering practice. As well as the more complex test cases considered, another contributing factor to the difference in studies is that in [40], a fixed number of eigenvectors was taken per subdomain (limiting the size of the coarse space), whereas here, eigenvalue thresholding was employed to provide a more robust approach, at the cost of a potentially larger coarse space. As such, the present study can be thought of as investigating the extent of what can be achieved in terms of a robust method in the ideal case, while [40] presents a viewpoint within the regime of more challenging practical problems. Identifying coarse spaces that can bridge this gap and provide a consistently robust approach even for the most demanding real-world applications remains an open area of research.

Author Contributions: Conceptualization, N.B. and V.D.; methodology, N.B.; software, N.B.; validation, N.B.; formal analysis, N.B. and V.D.; investigation, N.B.; resources, V.D.; writing—original draft preparation, N.B.; writing—review and editing, N.B. and V.D.; visualization, N.B.; supervision, V.D.; project administration, V.D.; funding acquisition, V.D. All authors have read and agreed to the published version of the manuscript.

Funding: This research was funded by EPSRC grant number EP/S004017/1.

Acknowledgments: Numerical results were obtained using the ARCHIE-WeSt High Performance Computer (www.archie-west.ac.uk accessed on 16 February 2022) based at the University of Strathclyde.

Conflicts of Interest: The authors declare no conflict of interest.

References

- Moiola, A.; Spence, E.A. Is the Helmholtz equation really sign-indefinite? *SIAM Rev.* **2014**, *56*, 274–312. [[CrossRef](#)]
- Ernst, O.G.; Gander, M.J. Why it is difficult to solve Helmholtz problems with classical iterative methods. In *Numerical Analysis of Multiscale Problems*; Graham, I.G., Hou, T.Y., Lakkis, O., Scheichl, R., Eds.; Springer: Berlin, Germany, 2012; pp. 325–363.
- Gander, M.J.; Zhang, H. A class of iterative solvers for the Helmholtz equation: Factorizations, sweeping preconditioners, source transfer, single layer potentials, polarized traces, and optimized Schwarz methods. *SIAM Rev.* **2019**, *60*, 3–76. [[CrossRef](#)]
- Gillman, A.; Barnett, A.H.; Martinsson, P.-G. A spectrally accurate direct solution technique for frequency-domain scattering problems with variable media. *BIT* **2015**, *55*, 141–170. [[CrossRef](#)]
- Wang, S.; de Hoop, M.V.; Xia, J. On 3D modeling of seismic wave propagation via a structured parallel multifrontal direct Helmholtz solver. *Geophys. Prospect.* **2011**, *59*, 857–873. [[CrossRef](#)]
- Calandra, H.; Gratton, S.; Pinel, X.; Vasseur, X. An improved two-grid preconditioner for the solution of three-dimensional Helmholtz problems in heterogeneous media. *Numer. Linear Algebra Appl.* **2013**, *20*, 663–688. [[CrossRef](#)]
- Hu, Q.; Zhang, H. Substructuring preconditioners for the systems arising from plane wave discretization of Helmholtz equations. *SIAM J. Sci. Comput.* **2016**, *38*, A2232–A2261. [[CrossRef](#)]
- Erlangga, Y.; Vuik, C.; Oosterlee, C. W. On a class of preconditioners for solving the Helmholtz equation. *Appl. Numer. Math.* **2004**, *50*, 409–425. [[CrossRef](#)]
- Erlangga, Y.; Oosterlee, C.W.; Vuik, C. A novel multigrid based preconditioner for heterogeneous Helmholtz problems. *SIAM J. Sci. Comput.* **2006**, *27*, 1471–1492. [[CrossRef](#)]
- Cocquet, P.-H.; Gander, M.J. How large a shift is needed in the shifted Helmholtz preconditioner for its effective inversion by multigrid? *SIAM J. Sci. Comput.* **2017**, *39*, A438–A478. [[CrossRef](#)]
- Dwarka, V.; Vuik, C. Scalable convergence using two-level deflation preconditioning for the Helmholtz equation. *SIAM J. Sci. Comput.* **2020**, *42*, A901–A928. [[CrossRef](#)]
- Lahaye, D.; Vuik, C. How to choose the shift in the shifted Laplace preconditioner for the Helmholtz equation combined with deflation. In *Modern Solvers for Helmholtz Problems*; Lahaye, D., Tang, J., Vuik, K., Eds.; Birkhäuser: Cham, Switzerland, 2017; pp. 85–112.
- Engquist, B.; Ying, L. Sweeping preconditioner for the Helmholtz equation: Hierarchical matrix representation. *Comm. Pure Appl. Math.* **2011**, *64*, 697–735. [[CrossRef](#)]
- Engquist, B.; Ying, L. Sweeping preconditioner for the Helmholtz equation: Moving perfectly matched layers. *Multiscale. Model. Simul.* **2011**, *9*, 686–710. [[CrossRef](#)]
- Taus, M.; Zepeda-Núñez, L.; Hewett, R.J.; Demanet, L. L-Sweeps: A scalable, parallel preconditioner for the high-frequency Helmholtz equation. *J. Comput. Phys.* **2020**, *420*, 109706. [[CrossRef](#)]
- Dai, R.; Modave, A.; Remacle, J.-F.; Geuzaine, C. Multidirectional sweeping preconditioners with non-overlapping checkerboard domain decomposition for Helmholtz problems. *J. Comput. Phys.* **2022**, *453*, 110887. [[CrossRef](#)]

17. Farhat, C.; Macedo, A.; Lesoinne, M. A two-level domain decomposition method for the iterative solution of high frequency exterior Helmholtz problems. *Numer. Math.* **2000**, *85*, 283–308. [[CrossRef](#)]
18. Farhat, C.; Avery, P.; Tezaur, R.; Li, J. FETI-DPH: A dual-primal domain decomposition method for acoustic scattering. *J. Comput. Acoust.* **2005**, *13*, 499–524. [[CrossRef](#)]
19. Després, B. Domain decomposition method for the Helmholtz problem. *C R Math. Acad. Sci. Paris I Math.* **1990**, *311*, 313–316.
20. Claeys, X.; Parolin, E. Robust treatment of cross points in Optimized Schwarz Methods. *arXiv* **2020**, arXiv:2003.06657.
21. Gander, M.J.; Magoules, F.; Nataf, F. Optimized Schwarz methods without overlap for the Helmholtz equation. *SIAM J. Sci. Comput.* **2002**, *24*, 38–60. [[CrossRef](#)]
22. Boubendir, Y.; Antoine, X.; Geuzaine, C. A quasi-optimal non-overlapping domain decomposition algorithm for the Helmholtz equation. *J. Comput. Phys.* **2012**, *231*, 262–280. [[CrossRef](#)]
23. Collino, F.; Ghanemi, S.; Joly, P. Domain decomposition method for harmonic wave propagation: A general presentation. *Comput. Methods Appl. Mech. Engrg.* **2000**, *184*, 171–211. [[CrossRef](#)]
24. Cai, X.-C.; Casarin, M.A.; Elliott, F.W., Jr.; Widlund, O.B. Overlapping Schwarz algorithms for solving Helmholtz's equation. *Contemp. Math.* **1998**, *218*, 391–399.
25. Gander, M.J.; Zhang, H. Optimized Schwarz methods with overlap for the Helmholtz equation. *SIAM J. Sci. Comput.* **2016**, *38*, A3195–A3219. [[CrossRef](#)]
26. Kimn, J.-H.; Sarkis, M. Restricted overlapping balancing domain decomposition methods and restricted coarse problems for the Helmholtz problem. *Comput. Methods Appl. Mech. Engrg.* **2007**, *196*, 1507–1514.
27. Graham, I.G.; Spence, E.A.; Vainikko, E. Recent results on domain decomposition preconditioning for the high-frequency Helmholtz equation using absorption. In *Modern Solvers for Helmholtz Problems*; Lahaye, D., Tang, J., Vuik, K., Eds.; Birkhäuser: Cham, Switzerland, 2017; pp. 3–26.
28. Kimn, J.-H.; Sarkis, M. Shifted Laplacian RAS solvers for the Helmholtz equation. In *Domain Decomposition Methods in Science and Engineering XX*; Bank, R., Holst, M., Widlund, O., Xu, J., Eds.; Springer: Berlin, Germany, 2013; pp. 151–158.
29. Graham, I.G.; Spence, E.A.; Vainikko, E. Domain decomposition preconditioning for high-frequency Helmholtz problems with absorption. *Math. Comp.* **2017**, *86*, 2089–2127. [[CrossRef](#)]
30. Graham, I.G.; Spence, E.A.; Zou, J. Domain Decomposition with local impedance conditions for the Helmholtz equation with absorption. *SIAM J. Numer. Anal.* **2020**, *58*, 2515–2543. [[CrossRef](#)]
31. Gong, S.; Graham, I.G.; Spence, E.A. Domain decomposition preconditioners for high-order discretizations of the heterogeneous Helmholtz equation. *IMA J. Numer. Anal.* **2021**, *41*, 2139–2185. [[CrossRef](#)]
32. Gong, S.; Gander, M.J.; Graham, I.G.; Lafontaine, D.; Spence, E.A. Convergence of parallel overlapping domain decomposition methods for the Helmholtz equation. *arXiv* **2021**, arXiv:2106.05218.
33. Bootland, N.; Dolean, V.; Kyriakis, A.; Pestana, J. Analysis of parallel Schwarz algorithms for time-harmonic problems using block Toeplitz matrices. *Electron. Trans. Numer. Anal.* **2022**, *55*, 112–141. [[CrossRef](#)]
34. Bonazzoli, M.; Dolean, V.; Graham, I.G.; Spence, E.A.; Tournier, P.-H. Domain decomposition preconditioning for the high-frequency time-harmonic Maxwell equations with absorption. *Math. Comp.* **2019**, *88*, 2559–2604. [[CrossRef](#)]
35. Spillane, N.; Dolean, V.; Hauret, P.; Nataf, F.; Pechstein, C.; Scheichl, R. Abstract robust coarse spaces for systems of PDEs via generalized eigenproblems in the overlaps. *Numer. Math.* **2014**, *126*, 741–770. [[CrossRef](#)]
36. Nataf, F.; Xiang, H.; Dolean, V.; Spillane, N. A coarse space construction based on local Dirichlet-to-Neumann maps. *SIAM J. Sci. Comput.* **2011**, *33*, 1623–1642. [[CrossRef](#)]
37. Bootland, N.; Dolean, V. On the Dirichlet-to-Neumann coarse space for solving the Helmholtz problem using domain decomposition. In *Numerical Mathematics and Advanced Applications ENUMATH 2019*; Vermolen, F.J., Vuik, C., Eds.; Springer: Cham, Switzerland, 2021; pp. 175–184.
38. Conen, L.; Dolean, V.; Krause, R.; Nataf, F. A coarse space for heterogeneous Helmholtz problems based on the Dirichlet-to-Neumann operator. *J. Comput. Appl. Math.* **2014**, *271*, 83–99. [[CrossRef](#)]
39. Bootland, N.; Dolean, V.; Graham, I.G.; Ma, C.; Scheichl, R. Overlapping Schwarz methods with GenEO coarse spaces for indefinite and non-self-adjoint problems. *arXiv* **2021**, arXiv:2110.13537.
40. Bootland, N.; Dolean, V.; Jolivet, P.; Tournier, P.-H. A comparison of coarse spaces for Helmholtz problems in the high frequency regime. *Comput. Math. Appl.* **2021**, *98*, 239–253. [[CrossRef](#)]
41. Zarmi, A.; Turkel, E. A general approach for high order absorbing boundary conditions for the Helmholtz equation. *J. Comput. Phys.* **2013**, *242*, 387–404. [[CrossRef](#)]
42. Beriot, H.; Modave, A. An automatic perfectly matched layer for acoustic finite element simulations in convex domains of general shape. *Int. J. Numer. Methods Energy* **2021**, *122*, 1239–1261. [[CrossRef](#)]
43. Harari, I.; Slavutin, M.; Turkel, E. Analytical and numerical studies of a finite element PML for the Helmholtz equation. *J. Comput. Acoust.* **2000**, *8*, 121–137. [[CrossRef](#)]
44. Babuska, I.M.; Sauter, S.A. Is the pollution effect of the FEM avoidable for the Helmholtz equation considering high wave numbers? *SIAM J. Numer. Anal.* **1997**, *34*, 2392–2423. [[CrossRef](#)]
45. Dolean, V.; Jolivet, P.; Nataf, F. *An Introduction to Domain Decomposition Methods: Algorithms, Theory, and Parallel Implementation*; Society for Industrial and Applied Mathematics (SIAM): Philadelphia, PA, USA, 2015.

46. Fish, J.; Qu, Y. Global-basis two-level method for indefinite systems. Part 1: Convergence studies. *Int. J. Numer. Methods Energy* **2000**, *49*, 439–460. [[CrossRef](#)]
47. Nataf, F.; Xiang, H.; Dolean, V. A two level domain decomposition preconditioner based on local Dirichlet-to-Neumann maps. *C R Math. Acad. Sci. Paris I Math.* **2010**, *348*, 1163–1167. [[CrossRef](#)]
48. Haferssas, R.; Jolivet, P.; Nataf, F. An additive Schwarz method type theory for Lions's algorithm and a symmetrized optimized restricted additive Schwarz method. *SIAM J. Sci. Comput.* **2017**, *39*, A1345–A1365. [[CrossRef](#)]
49. Nataf, F.; Tournier, P.-H. A GenEO domain decomposition method for saddle point problems. *arXiv* **2019**, arXiv:1911.01858.
50. Spillane, N. An abstract theory of domain decomposition methods with coarse spaces of the GenEO family. *arXiv* **2021**, arXiv:2104.00280.
51. Bootland, N.; Dolean, V.; Graham, I.G.; Ma, C.; Scheichl, R. GenEO coarse spaces for heterogeneous indefinite elliptic problems. In *Domain Decomposition Methods in Science and Engineering XXVI*; Brenner, S., Chung, E.T.S., Klawonn, A., Kwok, F., Xu, J., Zou, J., Eds.; Springer: Cham, Switzerland, 2017; *accepted*.
52. Hecht, F. New development in FreeFem++. *J. Numer. Math.* **2012**, *20*, 251–266. [[CrossRef](#)]
53. Lehoucq, R.B.; Sorensen, D.C.; Yang, C. *ARPACK Users' Guide: Solution of Large-Scale Eigenvalue Problems with Implicitly Restarted Arnoldi Methods*; Society for Industrial and Applied Mathematics (SIAM): Philadelphia, PA, USA, 1998.
54. Amestoy, P.R.; Duff, I.S.; L'Excellent, J.-Y.; Koster, J. A fully asynchronous multifrontal solver using distributed dynamic scheduling. *SIAM J. Matrix Anal. Appl.* **2001**, *23*, 15–41. [[CrossRef](#)]
55. Karypis, G.; Kumar, V. A fast and high quality multilevel scheme for partitioning irregular graphs. *SIAM J. Sci. Comput.* **1998**, *20*, 359–392. [[CrossRef](#)]